

# A Deterministic Multiscale Approach for Simulating Dilute Polymeric Fluids

David J. Knezevic and Endre Süli

**Abstract** We introduce a numerical method for solving the coupled Navier–Stokes–Fokker–Planck model (i.e. a micro–macro model) for dilute polymeric fluids where polymer molecules are modelled as FENE dumbbells. The Fokker–Planck equation is posed on a high-dimensional domain and is therefore challenging from a computational point of view. We summarise analytical results for a Galerkin spectral method for the Fokker–Planck equation in *configuration space*, before combining this method with a finite element scheme in *physical space* to obtain an alternating-direction method for the high-dimensional Fokker–Planck equation. Alternating-direction methods have been considered previously in the literature for this problem (e.g. by Chauvière & Lozinski); we present an alternative framework here that is underpinned by rigorous numerical analysis, and numerical results demonstrating the effectiveness of our approach. The algorithm is well suited to implementation on a parallel computer, and we exploit this fact to make large-scale computations feasible.

## 1 Introduction

In this paper we introduce a computational framework for solving the Navier–Stokes–Fokker–Planck system of partial differential equations (also known as the *micro–macro model*) that governs the evolution of a dilute suspension of dumbbells in a Newtonian solvent, which is a well-studied model of dilute polymeric fluids [3, 23]. We refer to the approach of directly solving the coupled Navier–Stokes–Fokker–Planck system as the *deterministic multiscale* method; this approach has recently been used successfully in a number of papers by Lozinski, Chauvière

---

E. Süli (✉)

OUCL, University of Oxford, Parks Road, Oxford, OX1 3QD, UK,

E-mail: endre.suli@comlab.ox.ac.uk

and collaborators (see [4, 5, 19]), although those authors did not consider rigorous numerical analysis of their algorithm – such analysis is a major emphasis in the present paper as well as in [14, 15]. It is worth highlighting at the outset that there is an extensive literature on numerical methods for this problem, but most of the previous work on the subject addresses either fully macroscopic models (such as the Olroyd-B model) in order to circumvent the multiscale nature of the Navier–Stokes–Fokker–Planck system (see the text [23] for an overview of this field) or uses a stochastic approach in which the micro–macro system is treated using Monte–Carlo-type methods (cf. [22]). Compared to a fully macroscopic approach, the primary advantage of the deterministic multiscale method is that it does not involve “closure approximations”; the shortcomings of such approximations are well documented [11, 17, 26]. Also, a possible drawback of the stochastic approach is the presence of slowly decaying stochastic error terms. Variance reduction techniques have been developed to minimise the impact of this stochastic error in Monte–Carlo-type methods; nevertheless, circumventing this error completely is an important motivation for moving to fully deterministic micro–macro methods. The drawback of the deterministic multiscale approach, however, is that (as we shall see below) the Fokker–Planck equation is posed on a high-dimensional domain, and therefore solving it using deterministic methods is an imposing challenge from the computational point of view. Following Chauvière & Lozinski, our approach is to use an alternating-direction scheme to ameliorate the “curse of dimensionality”, and we also use parallel computation to make large-scale simulations feasible in practice.

As indicated above, we are considering a dilute solution of microscopic dumbbells, i.e. two beads of small mass connected by a spring. The spring force law  $\underline{F}$  has a corresponding potential,  $U : \mathbb{R}_{\geq 0} \rightarrow \mathbb{R}$ , such that  $\underline{F}(\underline{q}) = U'(\frac{1}{2}|\underline{q}|^2)\underline{q}$ , where  $\underline{q} \in D$  is the *configuration* vector (or end-to-end vector) of a dumbbell. Here we consider the FENE force law [25], which, in non-dimensional form is:

$$U(\frac{1}{2}|\underline{q}|^2) := -\frac{b}{2} \ln \left( 1 - \frac{|\underline{q}|^2}{b} \right), \quad \underline{F}(\underline{q}) = \frac{\underline{q}}{1 - |\underline{q}|^2/b}, \quad (1)$$

where  $D = B(0, \sqrt{b}) \subset \mathbb{R}^d$ ,  $d = 2$  or  $3$ . We assume that  $b \in (2, \infty)$  (cf. [10] or Example 1.2 in [2]), and in practice  $b$  is typically chosen in the range [10, 100]. The theoretical results presented in this paper can be generalised to a broader class of FENE-like potentials that satisfy Hypotheses A and B from [15]. For simplicity of exposition, we restrict our attention to the FENE potential here.

Suppose the fluid is confined to a macroscopic physical domain  $\Omega$ , assumed to be a bounded open set in  $\mathbb{R}^d$ . Let  $\underline{u} : (\underline{x}, t) \in \Omega \times [0, T] \mapsto \underline{u}(\underline{x}, t) \in \mathbb{R}^d$  denote the macroscopic velocity field, and let  $p : (\underline{x}, t) \in \Omega \times [0, T] \mapsto p(\underline{x}, t) \in \mathbb{R}$  denote the pressure. It is typical in this problem to let  $\underline{\kappa}$  denote the macroscopic velocity gradient, i.e.  $\underline{\kappa} := \nabla_{\underline{x}} \underline{u}$ . Also, suppose the function  $(\underline{x}, \underline{q}, t) \mapsto \psi(\underline{x}, \underline{q}, t)$  represents the probability, at time  $t$ , of finding a dumbbell with center of mass in the volume element  $\underline{x} + d\underline{x}$  and orientation vector in the element  $\underline{q} + d\underline{q}$ . Then, for a

suspension of FENE dumbbells, we have the following system (in non-dimensional form):

$$\frac{\partial \underline{u}}{\partial t} + \underline{u} \cdot \nabla_x \underline{u} + \nabla_x p = \frac{\gamma}{\text{Re}} \Delta_x \underline{u} + \frac{b+d+2}{b} \frac{1-\gamma}{\text{Re Wi}} \nabla_x \cdot \underline{\tau}, \quad (2)$$

$$\nabla_x \cdot \underline{u} = 0, \quad (3)$$

$$\underline{\tau}(\underline{x}, t) = \int_D \underline{F} \otimes \underline{q} \psi(\underline{x}, \underline{q}, t) d\underline{q}, \quad (4)$$

for  $(\underline{x}, t) \in \Omega \times (0, T]$ , where  $\psi$  satisfies the Fokker–Planck equation:

$$\frac{\partial \psi}{\partial t} + \nabla_x \cdot (\underline{u} \psi) + \nabla_q \cdot (\underline{\kappa} \underline{q} \psi) = \frac{1}{2\text{Wi}} \nabla_q \cdot \left( M \nabla_q \left( \frac{\psi}{M} \right) \right), \quad (5)$$

or  $(\underline{x}, \underline{q}, t) \in \Omega \times D \times (0, T]$ . The system (2)–(5) is subject to the initial conditions:

$$\underline{u}(\underline{x}, 0) = \underline{u}_0(\underline{x}), \quad \underline{x} \in \Omega, \quad \psi(\underline{x}, \underline{q}, 0) = \psi_0(\underline{x}, \underline{q}), \quad (\underline{x}, \underline{q}) \in \Omega \times D. \quad (6)$$

In (2),  $\text{Re}$  is the Reynolds number,  $\text{Wi}$  is the Weissenberg number, which is the ratio of microscopic to macroscopic time-scales, and  $\gamma \in (0, 1)$  is the ratio of solvent viscosity to total viscosity. In (5),  $M$  is the (normalised) FENE *Maxwellian* defined by

$$\underline{q} \mapsto M(\underline{q}) := \frac{1}{Z} \exp\left(-U\left(\frac{1}{2}|\underline{q}|^2\right)\right) \in L^1(D), \quad Z := \int_D \exp\left(-U\left(\frac{1}{2}|\underline{q}|^2\right)\right) d\underline{q},$$

which, in the case of the FENE model, is  $M(\underline{q}) := \frac{1}{Z}(1 - |\underline{q}|^2/b)^{b/2}$ . In fact, the form of the Fokker–Planck equation given in (5) uses a Kolmogorov symmetrisation [16]; it is equivalent to the ‘standard’ form of the equation:

$$\frac{\partial \psi}{\partial t} + \nabla_x \cdot (\underline{u} \psi) + \nabla_q \cdot \left( \underline{\kappa} \underline{q} \psi - \frac{1}{2\text{Wi}} \underline{F}(\underline{q}) \psi \right) = \frac{1}{2\text{Wi}} \Delta_q \psi, \quad (7)$$

but from our point of view the advantage of (5) is that the unbounded convection coefficient ( $\underline{F}$  in (7)) is absorbed into a weighted diffusion term, which is convenient from the point of view of analysis. It should be noted, however, that in [5] Lozinski & Chauvière proposed a numerical method based on (7) in which the substitution  $\hat{\psi} := \psi/M^{2s/b}$  was used<sup>1</sup>; it was shown in Sect. 3.2 of [15] that with  $b \geq 4s^2/(2s-1)$  and  $s > 1/2$ , this also leads to a well-posed problem and a stable semidiscretisation in any number of space dimensions, and hence all of the analytical results developed in this paper could also be developed based on the Lozinski–Chauvière substitution. Nevertheless, the symmetry of (5) simplifies analysis of the numerical methods we consider, and therefore we focus on

<sup>1</sup> Based on computational experience, Lozinski & Chauvière recommended  $s = 2$  and  $s = 2.5$  for  $d = 2$  and  $d = 3$ , respectively.

the Maxwellian-transformed form of the Fokker–Planck equation in (5) for the remainder of this paper.

Since  $\psi$  is a probability density function (pdf) for each  $\underline{x} \in \Omega$ , the initial datum should be non-negative:

$$\psi(\underline{x}, \underline{q}, 0) = \psi_0(\underline{x}, \underline{q}) \geq 0, \quad \text{for a.e. } (\underline{x}, \underline{q}) \in \Omega \times D, \quad (8)$$

and should also satisfy the following normalisation property:

$$\int_D \psi_0(\underline{x}, \underline{q}) \, d\underline{q} = 1, \quad \text{for a.e. } \underline{x} \in \Omega. \quad (9)$$

It is crucial to note that (5) is posed in  $2d$  spatial dimensions, plus time. Since the computational complexity of standard numerical methods for PDEs grows exponentially with the dimension of the spatial domain, the high-dimensionality of (5) represents a significant computational challenge. Therefore, in a coupled algorithm for (2)–(6), solving the Fokker–Planck equation is generally the bottleneck step and as a result the focus of this paper is on the analysis and implementation of efficient numerical methods for (5).

In the papers of Lozinski, Chauvière et al. [4, 5, 18–20] and Helzel & Otto [9], the authors decomposed the differential operator  $L$  from (5) by defining  $L_x$  and  $L_q$  acting in the  $\underline{x}$ - and  $\underline{q}$ -direction, respectively. They then used an alternating-direction numerical method (also referred to as an operator-splitting or dimension-splitting approach) based on these operators.<sup>2</sup> We pursue the same approach in this paper and we shall survey a number of stability and convergence results that we proved for our computational framework in the papers [14, 15].

Note that the splitting introduced above leads to a sequence of  $d$ -dimensional solves at each time step rather than a single  $2d$ -dimensional solve. Also, this splitting of  $L$  allows different numerical methods to be used in  $\Omega$  and  $D$  (resulting in, what we call, a *heterogeneous* alternating-direction scheme). In Sect. 3 we consider heterogeneous alternating-direction numerical methods for the FENE Fokker–Planck equation on  $\Omega \times D$  based on a finite element method in  $\Omega$  and a single-domain Galerkin spectral method in  $D$ . These are appropriate choices because a finite element method is flexible enough to deal with the general domain  $\Omega$ , whereas  $D$  is always a ball in  $\mathbb{R}^d$ , and therefore the  $L_q$  operator is well suited to a spectral discretisation via a polar or spherical coordinate transformation to a cartesian product domain.

The structure of this paper is as follows. We begin in Sect. 2 with an overview of the analysis and implementation of a Galerkin spectral method for the Maxwellian-transformed Fokker–Planck equation in configuration space. This spectral method is then integrated into an alternating-direction scheme for the full Fokker–Planck equation on  $\Omega \times D$  in Sect. 3. Finally, we demonstrate the use of this alternating-direction scheme in an algorithm for the coupled Navier–Stokes–Fokker–Planck system for a channel flow problem of physical interest. We make concluding remarks in Sect. 5.

---

<sup>2</sup> These authors used (7), but the idea applies to (5) in the same way.

## 2 The Fokker–Planck Equation in Configuration Space

This section is concerned with the numerical approximation of the  $d$ -dimensional Fokker–Planck equation posed in configuration space:

$$\frac{\partial \psi}{\partial t} + \nabla_{\underline{q}} \cdot (\underline{\kappa} \underline{q} \psi) = \frac{1}{2\text{Wi}} \nabla_{\underline{q}} \cdot \left( M \nabla_{\underline{q}} \frac{\psi}{M} \right), \quad (\underline{q}, t) \in D \times (0, T], \quad (10)$$

where the  $d \times d$  tensor  $\underline{\kappa}$  is assumed to belong to  $(C[0, T])^{d \times d}$  (i.e. it is independent of  $\underline{x}$ ) and is such that  $\text{tr}(\underline{\kappa})(t) = 0$  for all  $t \in [0, T]$ . It will be assumed throughout that (10) is supplemented with the following initial and boundary conditions:

$$\psi(\underline{q}, 0) = \psi_0(\underline{q}), \quad \text{for all } \underline{q} \in D, \quad (11)$$

$$\psi(\underline{q}, t) = o\left(\sqrt{M(\underline{q})}\right), \quad \text{as } \text{dist}(\underline{q}, \partial D) \rightarrow 0_+, \text{ for all } t \in (0, T]. \quad (12)$$

As in (8) and (9), the initial datum  $\psi_0$  is such that  $\psi_0 \geq 0$  and  $\int_D \psi_0(\underline{q}) \, d\underline{q} = 1$ .

The motivation for studying this subproblem is that, as indicated in Sect. 1, an efficient approach to the numerical solution of (5) in  $2d + 1$  variables is based on operator-splitting with respect to  $(\underline{q}, t)$  and  $(\underline{x}, t)$ . Thereby, the resulting time-dependent transport equation with respect to  $(\underline{x}, t)$  is completely standard,  $\psi_t + \nabla_{\underline{x}} \cdot (\underline{u}(\underline{x}, t)\psi) = 0$ , while the transport-diffusion equation with respect to  $(\underline{q}, t)$  is (10).

### 2.1 Weak Formulation and Backward Euler Semidiscretisation

Following [15], let  $\hat{\varphi} := \frac{\varphi}{\sqrt{M}}$  and  $\nabla_M \hat{\varphi} := \sqrt{M} \nabla_{\underline{q}} \left( \frac{\hat{\varphi}}{\sqrt{M}} \right)$ , and define the function space  $H_0^1(D; M)$  to be the closure of  $C_0^\infty(D)$  in the norm of  $H^1(D; M)$ , and

$$H^1(D; M) := \left\{ \zeta \in L^2(D) : \|\zeta\|_{H^1(D; M)}^2 := \int_D \left( |\zeta|^2 + |\nabla_M \zeta|^2 \right) \, d\underline{q} < \infty \right\}.$$

Then, (10) has the following weak formulation. Given  $\hat{\psi}_0 := \psi_0 / \sqrt{M} \in L^2(D)$ , find  $\hat{\psi} \in L^\infty(0, T; L^2(D)) \cap L^2(0, T; H_0^1(D; M))$  such that

$$\frac{d}{dt} \int_D \hat{\psi} \hat{\varphi} \, d\underline{q} - \int_D \underline{\kappa} \underline{q} \hat{\psi} \cdot \nabla_M \hat{\varphi} \, d\underline{q} + \frac{1}{2\text{Wi}} \int_D \nabla_M \hat{\psi} \cdot \nabla_M \hat{\varphi} \, d\underline{q} = 0, \quad (13)$$

for all  $\hat{\varphi} \in H_0^1(D; M)$  in the sense of distributions on  $(0, T)$ , and  $\hat{\psi}(\cdot, 0) = \hat{\psi}_0(\cdot)$ . Notice that we solve for  $\hat{\psi}$ ;  $\psi$  is recovered by setting  $\psi := \sqrt{M} \hat{\psi}$ . The Lozinski–Chauvière substitution introduced in Sect. 1 is identical to the substitution  $\psi := \sqrt{M} \hat{\psi}$  in the case that  $s = b/4$ .

It is shown in Sect. 2 of [15] that  $H^1(D; M) = H_0^1(D; M)$  and  $H_0^1(D) \subset H_0^1(D; M)$ .<sup>3</sup> The connection between  $H_0^1(D; M)$  and  $H_0^1(D)$  will prove helpful in the development of Galerkin methods for (13), since the construction of finite-dimensional subspaces of  $H_0^1(D)$  and the analysis of their approximation properties are well understood.

In [15], the following backward-Euler semidiscretisation of (13) was studied in detail: Let  $N_T \geq 1$  be an integer,  $\Delta t = T/N_T$ , and  $t^n = n\Delta t$ , for  $n = 0, 1, \dots, N_T$ . Discretising (13) in time using the backward Euler method yields the following semi-discrete numerical scheme.

Given  $\hat{\psi}^0 := \hat{\psi}_0 = \psi_0/\sqrt{M} \in L^2(D)$ , find  $\hat{\psi}^{n+1} \in H_0^1(D; M)$ ,  $n = 0, \dots, N_T - 1$ , such that

$$\int_D \frac{\hat{\psi}^{n+1} - \hat{\psi}^n}{\Delta t} \hat{\phi} \, d\mathbf{q} - \int_D (\kappa^{n+1} \underline{q} \hat{\psi}^{n+1}) \cdot \underline{\nabla}_M \hat{\phi} \, d\mathbf{q} + \frac{1}{2\text{Wi}} \int_D \underline{\nabla}_M \hat{\psi}^{n+1} \cdot \underline{\nabla}_M \hat{\phi} \, d\mathbf{q} = 0,$$

for all  $\hat{\phi} \in H_0^1(D; M)$ .

The following stability lemma for (14) was proved in Sect. 3 of [15].

**Lemma 1.** *Let  $\Delta t = T/N_T$ ,  $N_T \geq 1$ ,  $\kappa \in (C[0, T])^{d \times d}$ ,  $\hat{\psi}^0 \in L^2(D)$ , and define  $c_0 := 1 + 4\text{Wi}b \|\kappa\|_{L^\infty(0, T)}^2$ . If  $\Delta t$  is such that  $0 < c_0 \Delta t \leq 1/2$ , then we have, for all  $m$  such that  $1 \leq m \leq N_T$ ,*

$$\|\hat{\psi}^m\|^2 + \sum_{n=0}^{m-1} \Delta t \left\| \frac{\hat{\psi}^{n+1} - \hat{\psi}^n}{\sqrt{\Delta t}} \right\|^2 + \sum_{n=0}^{m-1} \frac{\Delta t}{2\text{Wi}} \|\underline{\nabla}_M \hat{\psi}^{n+1}\|^2 \leq e^{2c_0 m \Delta t} \|\hat{\psi}^0\|^2.$$

Also, the existence and uniqueness of a weak solution of (13) was established in Theorem 3.2 of [15]. The proof makes use of the stability result in Lemma 1 in order to use compactness results for the bounded sequence of solutions to (14) as  $\Delta t \rightarrow 0_+$ .

## 2.2 Fully-Discrete Spectral Method

Let  $\mathcal{P}_N(D)$  be a finite-dimensional subspace of  $H_0^1(D; M)$ , to be chosen below, and let  $\hat{\psi}_N^n \in \mathcal{P}_N(D)$  be the solution at time level  $n$  of our fully-discrete Galerkin method:

$$\int_D \frac{\hat{\psi}_N^{n+1} - \hat{\psi}_N^n}{\Delta t} \hat{\phi} \, d\mathbf{q} - \int_D (\kappa^{n+1} \underline{q} \hat{\psi}_N^{n+1}) \cdot \underline{\nabla}_M \hat{\phi} \, d\mathbf{q} + \frac{1}{2\text{Wi}} \int_D \underline{\nabla}_M \hat{\psi}_N^{n+1} \cdot \underline{\nabla}_M \hat{\phi} \, d\mathbf{q} = 0 \quad \forall \hat{\phi} \in \mathcal{P}_N(D), \quad n = 0, \dots, N_T - 1, \quad (14)$$

$$\hat{\psi}_N^0(\cdot) := \text{the } L^2(D) \text{ orthogonal projection of } \hat{\psi}_0(\cdot) = \hat{\psi}(\cdot, 0) \text{ onto } \mathcal{P}_N(D). \quad (15)$$

<sup>3</sup> In fact, these results hold for all FENE-like potentials, cf. Sect. 1.

The case  $D \subset \mathbb{R}^2$  was considered in detail in [15]. Suppose we transform  $D$  into the rectangle  $(r, \theta) \in R := (0, 1) \times (0, 2\pi)$  using the polar coordinate transformation  $q = (q_1, q_2) = (\sqrt{br} \cos \theta, \sqrt{br} \sin \theta)$ . Also, suppose that  $\hat{\psi} \in \mathbf{H}_0^1(D)$  and let  $\tilde{\psi}(r, \theta) := \hat{\psi}(q_1, q_2)$ . It was proved in Lemma 5.2 of [15] that  $\tilde{\psi}$  can be written in polar coordinates as follows:

$$\tilde{\psi}(r, \theta) = \tilde{\psi}_1(r) + r\tilde{\psi}_2(r, \theta), \quad (r, \theta) \in R = (0, 1) \times (0, 2\pi). \quad (16)$$

Using the structure in (16), we defined in [15] the spectral basis  $\mathcal{A}$  as  $\mathcal{A} := \mathcal{A}_1 \cup \mathcal{A}_2$  where:

$$\begin{aligned} \mathcal{A}_1 &:= \{(1-r)P_k(r) : k = 0, \dots, N_r - 1\}, \\ \mathcal{A}_2 &:= \{r(1-r)P_k(r)\Phi_{il}(\theta) : k = 0, \dots, N_r - 1; i = 0, 1; l = 1, \dots, N_\theta\}. \end{aligned}$$

$P_k$  is a polynomial of degree  $k$  in  $r \in [0, 1]$  and  $\Phi_{il}(\theta) = (1-i)\cos(2l\theta) + i\sin(2l\theta)$ ,  $\theta \in [0, \pi]$ . Notice that the polynomials in both  $\mathcal{A}_1$  and  $\mathcal{A}_2$  contain the factor  $(1-r)$  in order to impose the homogeneous Dirichlet boundary condition on  $\partial D$ . Basis  $\mathcal{A}$  is defined in order to mimic the decomposition (16) of the weak solution  $\tilde{\psi}$  in polar coordinates: the role of  $\text{span}(\mathcal{A}_1)$  is to approximate  $\tilde{\psi}_1$  while  $\text{span}(\mathcal{A}_2)$  is meant to approximate  $r\tilde{\psi}_2$ .

Now, let  $\mathcal{P}_N(D)$  be  $\text{span}(\mathcal{A})$  defined from  $R$  to  $D$ . Approximation results were derived for this discrete space in Sect. 5 of [15], which enabled the derivation of the following optimal order spectral convergence estimate for the fully-discrete spectral method (14)–(15): for  $\hat{\psi} \in \mathcal{H}^{k+1, l+1}(D)$  with  $k, l \geq 1$  we have,

$$\begin{aligned} &\|\hat{\psi} - \hat{\psi}_N\|_{\ell^\infty(0, T; L^2(D))} + \|\tilde{\nabla}_M(\hat{\psi} - \hat{\psi}_N)\|_{\ell^2(0, T; L^2(D))} \\ &\leq C_1 N_r^{-k} \left( \|\hat{\psi}\|_{\ell^\infty(0, T; \mathcal{H}_r^k(D))} + \|\hat{\psi}\|_{\ell^2(0, T; \mathcal{H}_r^{k+1}(D))} + \left\| \frac{\partial \hat{\psi}}{\partial t} \right\|_{L^2(0, T; \mathcal{H}_r^k(D))} \right) \\ &\quad + C_2 N_\theta^{-l} \left( \|\hat{\psi}\|_{\ell^\infty(0, T; \mathcal{H}_\theta^l(D))} + \|\hat{\psi}\|_{\ell^2(0, T; \mathcal{H}_\theta^{l+1}(D))} + \left\| \frac{\partial \hat{\psi}}{\partial t} \right\|_{L^2(0, T; \mathcal{H}_\theta^l(D))} \right) \\ &\quad + C_3 \Delta t \left\| \frac{\partial^2 \hat{\psi}}{\partial t^2} \right\|_{L^2(0, T; L^2(D))}, \end{aligned} \quad (17)$$

(see Sect. 5 of [15] for definitions of the non-standard Sobolev spaces  $\mathcal{H}^{k+1, l+1}(D)$ ,  $\mathcal{H}_r^k(D)$  and  $\mathcal{H}_\theta^l(D)$ ).

Note that we also considered a second basis,  $\mathcal{B}$ , in [15], proposed by Matsushima & Marcus [21] and Verkley [24], which satisfies the full pole condition on  $D$  (cf. [7]), and therefore the space defined by  $\mathcal{B}$  is contained in  $C^\infty(\bar{D}) \cap C_0(D)$ . The numerical method based on  $\mathcal{B}$  was found to be more efficient in practice than the one based on  $\mathcal{A}$  for the FENE Fokker–Planck equation on  $D$  since  $\hat{\psi}$  is typically

very smooth. Finally, we considered a basis in [14] in the case of  $d = 3$ , referred to as basis  $\mathcal{C}$ , which, following [4], was defined as follows:

$$\mathcal{C} := \{Y_{lm}^{ik} : 0 \leq k \leq N_r - 1, i \in \{0, 1\}, l \in \{0, 2, 4, \dots, N_{\text{sph}}\} \text{ and } i \leq m \leq l\},$$

where  $Y_{lm}^{ik}(r, \theta, \phi) := (1 - r)Q_k(r)S_{l,m}^i(\theta, \phi)$ , and the  $S_{l,m}^i$  are spherical harmonics:  $S_{l,m}^i(\theta, \phi) := C(l, m)P_l^m(\cos \phi)((1 - i)\cos(m\theta) + i\sin(m\theta))$ . Note that we showed in [14] that a splitting of the form (16) is not required in the case of  $d = 3$ .

A range of numerical results for spectral methods based on  $\mathcal{A}$  and  $\mathcal{B}$  in the case of  $d = 2$  were presented in Sect. 7 of [15], and the convergence behaviour we obtained in practice was consistent with (17). The numerical method based on  $\mathcal{C}$  is completely analogous, and it was shown in Sect. 2.6.3 of [13] that the convergence behaviour of this method in three dimensions is essentially the same as for methods  $\mathcal{A}$  and  $\mathcal{B}$  in two dimensions.

### 3 An Alternating-Direction Scheme for the Full Fokker–Planck Equation

In this section, we describe numerical methods for the Maxwellian-transformed Fokker–Planck equation posed on  $\Omega \times D \times (0, T]$ . Here we assume that  $\underline{u}$  is an *a priori* defined velocity field. Once the numerical scheme for the Fokker–Planck equation with a given  $\underline{u}$  is understood, it is straightforward to couple to the Navier–Stokes equations. These methods build upon the  $\underline{q}$ -direction spectral method introduced in Sect. 2. In this case, the weak formulation is as follows: Given  $\hat{\psi}_0 \in L^2(\Omega \times D)$ , find  $\hat{\psi} \in L^\infty(0, T; L^2(\Omega \times D)) \cap L^2(0, T; \mathcal{X})$  such that

$$\begin{aligned} \hat{\psi}(\underline{x}, \underline{q}, 0) &= \hat{\psi}_0(\underline{x}, \underline{q}), \quad (\underline{x}, \underline{q}) \in \Omega \times D, \\ \frac{d}{dt}(\hat{\psi}, \xi) + (\underline{u} \cdot \nabla_{\underline{x}} \hat{\psi}, \xi) - (\kappa \underline{q} \hat{\psi}, \nabla_M \xi) + \frac{1}{2\text{Wi}} (\nabla_M \hat{\psi}, \nabla_M \xi) &= 0 \quad \forall \xi \in \mathcal{X}, \end{aligned}$$

in the sense of distributions on  $(0, T)$ , and again  $\psi$  is recovered by multiplying  $\hat{\psi}$  by  $\sqrt{M}$ . Following Sect. 2, we impose a zero Dirichlet boundary condition on  $\Omega \times \partial D$  for  $t \in (0, T]$ . See [14] for the hypotheses on  $\underline{u}$  and for the definition of the space  $\mathcal{X}$ .

The alternating-direction method under consideration here is nonstandard in the sense that we consider  $d$ -dimensional cross-sections (rather than one-dimensional cross-sections) of  $\Omega \times D$ . This leads to a formidable computational challenge because we typically need to solve a large number of problems posed in  $d$  spatial dimensions in each time-step. However, the method is extremely well suited to implementation on a parallel architecture since the  $\underline{q}$ -direction solves are completely independent from one another, and similarly the  $\underline{x}$ -direction solves are decoupled also. Our computational results in Sect. 4 were obtained using a parallel implementation of the alternating-direction methods described here.

### 3.1 The Alternating-Direction Methods

We now introduce the alternating-direction Galerkin methods for the weak formulation given above. These algorithms combine a classical Douglas–Dupont-type alternating-direction scheme [6] in the  $\underline{x}$ -direction, with a new quadrature-based scheme in the  $\underline{q}$ -direction.

First of all, define the bases

$$\{Y_k \in \mathcal{P}_N(D) : 1 \leq k \leq N_D\} \quad \text{and} \quad \{X_i \in V_h : 1 \leq i \leq N_\Omega\}, \quad (18)$$

such that  $\text{span}(\{Y_k\}_{1 \leq k \leq N_D}) = \mathcal{P}_N(D)$  and  $\text{span}(\{X_i\}_{1 \leq i \leq N_\Omega}) = V_h$ , where  $V_h$  is an  $H^1(\Omega)$ -conforming finite element space based on a mesh  $\mathcal{T}_h$  of  $\overline{\Omega}$ . Let  $\hat{\psi}_{h,N}$  denote our discrete solution, such that  $\hat{\psi}_{h,N} \in V_h \otimes \mathcal{P}_N(D)$ .

Also, we need to specify a quadrature rule on  $\Omega$ . Let  $\{\underline{x}_m, w_m\}$ ,  $w_m > 0$ ,  $\underline{x}_m \in \overline{\Omega}$ ,  $m = 1, \dots, Q_\Omega$  define an element-based quadrature rule on  $\mathcal{T}_h$ , where the  $\underline{x}_m$  are the quadrature points and the  $w_m$  are the corresponding weights. Therefore, for functions  $f, g \in C^0(\overline{\Omega})$ , the quadrature sum is evaluated element-wise as follows,

$$\sum_{m=1}^{Q_\Omega} w_m f(\underline{x}_m) g(\underline{x}_m) = \sum_{K \in \mathcal{T}_h} \sum_{l=1}^{Q_K} w_l^K f(\underline{x}_l^K) g(\underline{x}_l^K), \quad (19)$$

where  $Q_K$  is the number of quadrature points in element  $K$ . In [14], we introduced hypotheses on this quadrature rule that are necessary for our numerical analysis; we refer the reader to that paper for more details. The idea of using this quadrature rule in the context of the alternating-direction scheme is that by performing the  $\underline{q}$ -direction solves at quadrature points  $\underline{x}_m$  we are able to recover a Galerkin formulation for the numerical method on  $\Omega \times D$ .

Noting that  $\hat{\psi}_{h,N}$  can be written in terms of the coefficients  $\{\hat{\psi}_{ik}\}$  as  $\hat{\psi}_{h,N} := \sum_{i=1}^{N_\Omega} \sum_{k=1}^{N_D} \hat{\psi}_{ik} X_i Y_k \in V_h \otimes \mathcal{P}_N(D)$ , we define the *line functions*,  $\hat{\psi}_k$ , for  $k = 1, \dots, N_D$ , by  $\hat{\psi}_k := \sum_{i=1}^{N_\Omega} \hat{\psi}_{ik} X_i \in V_h$ . Then we have  $\hat{\psi}_{h,N}(\underline{x}, \underline{q}) = \sum_{k=1}^{N_D} \hat{\psi}_k(\underline{x}) Y_k(\underline{q})$ . These formulas shall be useful in the discussion of the alternating-direction methods below.

We now define two alternating-direction methods, referred to as method I and method II. The distinction between these schemes is that method I uses a semi-implicit spectral method in the  $\underline{q}$ -direction (i.e. the term containing  $\kappa$  is treated explicitly in time) whereas method II uses a fully-implicit temporal discretisation.

*Method I: Semi-implicit scheme.* Method I is initialised by computing the  $L^2(\Omega \times D)$  projection of the initial datum  $\hat{\psi}_0 \in L^2(\Omega \times D)$  onto  $V_h \otimes \mathcal{P}_N(D)$ , so that  $\hat{\psi}_{h,N}^0 \in V_h \otimes \mathcal{P}_N(D)$  satisfies

$$\left( \hat{\psi}_0, \zeta \right) = \left( \hat{\psi}_{h,N}^0, \zeta \right) \quad \text{for all } \zeta \in V_h \otimes \mathcal{P}_N(D). \quad (20)$$

Then, the alternating-direction method consists of two stages at each time-step: the  $\underline{q}$ -direction stage and the  $\underline{x}$ -direction stage. We begin with the  $\underline{q}$ -direction stage, which essentially uses the Galerkin spectral method in  $D$  from Sect. 2.

Suppose  $\hat{\psi}_{h,N}^n \in V_h \otimes \mathcal{P}_N(D)$ . Then, in the  $\underline{q}$ -direction stage we compute  $\hat{\psi}_{h,N}^{n*}(\underline{x}_m, \cdot) \in \mathcal{P}_N(D)$  for each  $m = 1, \dots, Q_\Omega$  satisfying

$$\begin{aligned} & \int_D \frac{\hat{\psi}_{h,N}^{n*}(\underline{x}_m, \underline{q}) - \hat{\psi}_{h,N}^n(\underline{x}_m, \underline{q})}{\Delta t} Y_l(\underline{q}) \, d\underline{q} \\ & + \frac{1}{2\text{Wi}} \int_D \nabla_M \hat{\psi}_{h,N}^{n*}(\underline{x}_m, \underline{q}) \cdot \nabla_M Y_l(\underline{q}) \, d\underline{q} \\ & = \int_D (\kappa^n(\underline{x}_m) \underline{q} \hat{\psi}_{h,N}^n(\underline{x}_m, \underline{q})) \cdot \nabla_M Y_l(\underline{q}) \, d\underline{q}, \end{aligned} \quad (21)$$

for  $l = 1, \dots, N_D$ . In order to separate out the  $\underline{x}$ - and  $\underline{q}$ -direction dependencies more clearly, we rewrite this equation in terms of line functions, i.e.:

$$\begin{aligned} & \sum_{k=1}^{N_D} \hat{\psi}_k^{n*}(\underline{x}_m) \left( \int_D Y_k(\underline{q}) Y_l(\underline{q}) \, d\underline{q} + \frac{\Delta t}{2\text{Wi}} \int_D \nabla_M Y_k(\underline{q}) \cdot \nabla_M Y_l(\underline{q}) \, d\underline{q} \right) \\ & = \sum_{k=1}^{N_D} \hat{\psi}_k^n(\underline{x}_m) \left( \int_D Y_k(\underline{q}) Y_l(\underline{q}) \, d\underline{q} + \Delta t \int_D (\kappa^n(\underline{x}_m) \underline{q} Y_k(\underline{q})) \cdot \nabla_M Y_l(\underline{q}) \, d\underline{q} \right), \end{aligned} \quad (22)$$

for  $l = 1, \dots, N_D$ . This system is solved at each quadrature point  $\underline{x}_m$ ,  $m = 1, \dots, Q_\Omega$ , and the linear solves are completely independent from one another. This independence enables parallel computation to be used very effectively in this context.

The  $\underline{q}$ -direction stage is complete once the values  $\psi_k^{n*}(\underline{x}_m)$ ,  $k = 1, \dots, N_D$ ,  $m = 1, \dots, Q_\Omega$ , have been computed, and then we can begin solving in the  $\underline{x}$ -direction. In the  $\underline{x}$ -direction stage, we use a finite element discretisation of the transport equation,  $\psi_t + \nabla_x \cdot (\underline{u}(\underline{x}, t)\psi) = 0$ , to update the output data from the  $\underline{q}$ -direction stage. That is, for a given  $k$ , we find  $\hat{\psi}_k^{n+1} \in V_h$ , satisfying:

$$\int_\Omega \hat{\psi}_k^{n+1} X_i \, d\underline{x} + \Delta t \int_\Omega (\underline{u}^{n+1} \cdot \nabla_x \hat{\psi}_k^{n+1}) X_i \, d\underline{x} = \sum_{m=1}^{Q_\Omega} w_m \hat{\psi}_k^{n*}(\underline{x}_m) X_i(\underline{x}_m), \quad (23)$$

for  $i = 1, \dots, N_\Omega$ , and, just as in the  $\underline{q}$ -direction, these computations are decoupled from one another.

Once the  $\underline{x}$ -direction computations are complete, we have the numerical solution at time level  $n+1$ :  $\hat{\psi}_{h,N}^{n+1} = \sum_{k=1}^{N_D} \hat{\psi}_k^{n+1} Y_k \in V_h \otimes \mathcal{P}_N(D)$ . Hence method I is defined by the initialisation (20), the  $\underline{q}$ -direction spectral method (22) and the  $\underline{x}$ -direction finite element method (23). In Lemma 3.2 of [14] we show that method I

is equivalent to a one-step Galerkin formulation on  $\Omega \times D$ . This equivalent one-step formulation allows standard tools of numerical analysis to be applied to explore the stability and convergence properties of this method.

*Method II: Fully-implicit scheme.* Method II is very similar to method I, the sole difference being that the term containing  $\underline{\kappa}$  is now treated implicitly in time.

Using the line function notation of (22), the  $\underline{q}$ -direction numerical method is defined as follows: Given the line functions  $\hat{\psi}_k^n \in V_h$ ,  $k = 1, \dots, N_D$ , determine the values  $\hat{\psi}_k^{n*}(\underline{x}_m)$  satisfying

$$\begin{aligned} \sum_{k=1}^{N_D} \hat{\psi}_k^{n*}(\underline{x}_m) \left( \int_D Y_k(\underline{q}) Y_l(\underline{q}) \, d\underline{q} + \frac{\Delta t}{2\mathbb{W}i} \int_D \nabla_M Y_k(\underline{q}) \cdot \nabla_M Y_l(\underline{q}) \, d\underline{q} \right. \\ \left. - \Delta t \int_D (\underline{\kappa}^{n+1}(\underline{x}_m) \underline{q} Y_k(\underline{q})) \cdot \nabla_M Y_l(\underline{q}) \, d\underline{q} \right) = \sum_{k=1}^{N_D} \hat{\psi}_k^n(\underline{x}_m) \int_D Y_k(\underline{q}) Y_l(\underline{q}) \, d\underline{q}, \end{aligned} \quad (24)$$

for all  $l = 1, \dots, N_D$ , and for each quadrature point  $\underline{x}_m$ ,  $m = 1, \dots, Q_\Omega$ .

The initialisation and  $\underline{x}$ -direction stages for method II are identical to those given for method I, hence we omit them here.

Clearly methods I and II are closely related to one another. Note, however, that from a practical point of view there is a trade-off in computational efficiency between the two methods because, on the one hand, method I requires less computation per time-step, since the matrix for the  $\underline{q}$ -direction linear systems can be pre-assembled and LU-factorised only once since it is independent of  $\underline{\kappa}$ , whereas the  $\underline{q}$ -direction matrix for method II must be reassembled at each quadrature point. On the other hand, however, the fully implicit temporal discretisation used by method II tends to be more tolerant of large time-step sizes and coarse spatial discretisations than the semi-implicit scheme of method I, especially for larger flow rates and Weissenberg numbers (e.g. see Sect. 2.6.2 of [13]).

An important difference between methods I and II from the analytical point of view is that there is no equivalent one-step formulation available for method II. In [14], we proved stability and convergence results for method I based on its equivalent one-step formulation. That is, with some assumptions on the  $\underline{x}$ -direction quadrature rule, we established stability results of the form of Lemma 1 for method I and, supposing that the set of shape functions for each element in  $\mathcal{T}_h$  contains all polynomials of degree less than  $s + 1$ , we then proved the following error estimate for method I:

$$\begin{aligned} & \|\hat{\psi} - \hat{\psi}_{h,N}\|_{\ell^\infty(0,T;L^2(\Omega \times D))} + \|\nabla_M(\hat{\psi} - \hat{\psi}_{h,N})\|_{\ell^2(0,T;L^2(\Omega \times D))} \\ & \leq C_1 h^s \left( \|\hat{\psi}\|_{\ell^\infty(0,T;H^s(\Omega;L^2(D)))} + \left\| \frac{\partial \hat{\psi}}{\partial t} \right\|_{L^2(0,T;H^s(\Omega;L^2(D)))} \right) \\ & \quad + \left\| \hat{\psi} \right\|_{\ell^2(0,T;H^s(\Omega;H_0^1(D;M)))} + \left\| \hat{\psi} \right\|_{\ell^2(0,T;H^{s+1}(\Omega;L^2(D)))} \end{aligned}$$

$$\begin{aligned}
& + C_2 N_r^{-k} \left( \|\hat{\psi}\|_{\ell^\infty(0,T;L^2(\Omega;\mathcal{H}_r^k(D)))} + \left\| \frac{\partial \hat{\psi}}{\partial t} \right\|_{L^2(0,T;L^2(\Omega;\mathcal{H}_r^k(D)))} \right. \\
& \quad \left. + \|\hat{\psi}\|_{\ell^2(0,T;H^1(\Omega;\mathcal{H}_r^k(D)))} + \|\hat{\psi}\|_{\ell^2(0,T;L^2(\Omega;\mathcal{H}_r^{k+1}(D)))} \right) \\
& + C_3 N_\theta^{-l} \left( \|\hat{\psi}\|_{\ell^\infty(0,T;L^2(\Omega;\mathcal{H}_\theta^l(D)))} + \left\| \frac{\partial \hat{\psi}}{\partial t} \right\|_{L^2(0,T;L^2(\Omega;\mathcal{H}_\theta^l(D)))} \right. \\
& \quad \left. + \|\hat{\psi}\|_{\ell^2(0,T;H^1(\Omega;\mathcal{H}_\theta^l(D)))} + \|\hat{\psi}\|_{\ell^2(0,T;L^2(\Omega;\mathcal{H}_\theta^{l+1}(D)))} \right) \\
& + C_4 \Delta t \left( \|\hat{\psi}\|_{\ell^2(0,T;L^2(\Omega \times D))} + \|\hat{\psi}\|_{H^2(0,T;L^2(\Omega \times D))} + \|\nabla_x \nabla_M \hat{\psi}\|_{\ell^2(0,T;L^2(\Omega \times D))} \right. \\
& \quad \left. + N_r^{-k} \|\hat{\psi}\|_{\ell^2(0,T;H^1(\Omega;\mathcal{H}_r^{k+1}(D)))} + N_\theta^{-l} \|\hat{\psi}\|_{\ell^2(0,T;H^1(\Omega;\mathcal{H}_\theta^{l+1}(D)))} \right). \tag{25}
\end{aligned}$$

This error bound assumes that basis  $\mathcal{A}$  is used for the  $q$ -direction spectral method; it would be straightforward (but laborious) to extend (25) to bases  $\mathcal{B}$  or  $\mathcal{C}$  introduced in Sect. 2.

We could not apply the same convergence argument to method II due to the absence of an equivalent one-step formulation; nevertheless, in Lemma 3.4 of [14], we proved the unconditional stability of method II.

## 4 The Micro–Macro Model

We now present some numerical results for a channel flow problem using a coupled algorithm for the Navier–Stokes–Fokker–Planck system (2)–(6) (see [14] for other computational results using the same approach, including a computation in the  $d = 3$  case). We implemented the Navier–Stokes solver using a Taylor–Hood mixed finite element method [8] in the free C++ finite element library `libMesh` [12]. We used a finite element space of continuous piecewise quadratic functions for  $V_h$ , and  $V_h$  was also used as the velocity space in the Taylor–Hood method, hence  $\underline{u}_h$ , the finite element approximation to  $\underline{u}$ , belongs to  $(V_h)^d$ . The alternating-direction method was implemented for parallel computation; the  $q$ -direction spectral method was implemented in `PETSc` [1] and `libMesh` was used for the  $x$ -direction finite element method (see [14] for more details of the implementation).

We considered a planar flow around a cylindrical obstacle in a channel. This is a standard benchmark problem in the polymer fluids literature (cf. Chap. 9 of [23]) and was also considered using deterministic multiscale methods by Chauvière & Lozinski in [4, 5, 19]. In the computation presented here,  $\mathcal{T}_h$  contained 1505 triangular finite elements and  $Q_\Omega = 9030$ . For the  $q$ -direction spectral method we used basis  $\mathcal{A}$ . We imposed a parabolic inflow velocity profile for  $\underline{u}$  on the left boundary of  $\Omega$  with  $U_{\max} = 1$ , a Neumann condition on the right boundary, a no-slip condition ( $\underline{u} = \underline{0}$ ) for the obstacle and top boundary, and a symmetry condition on the bottom boundary. We used the parameters  $b = 12$ ,  $\gamma = 0.59$ ,  $\text{Re} = 1$  and we considered two choices of the Weissenberg number, (1)  $\text{Wi} = 1$  and (2)  $\text{Wi} = 3$ .

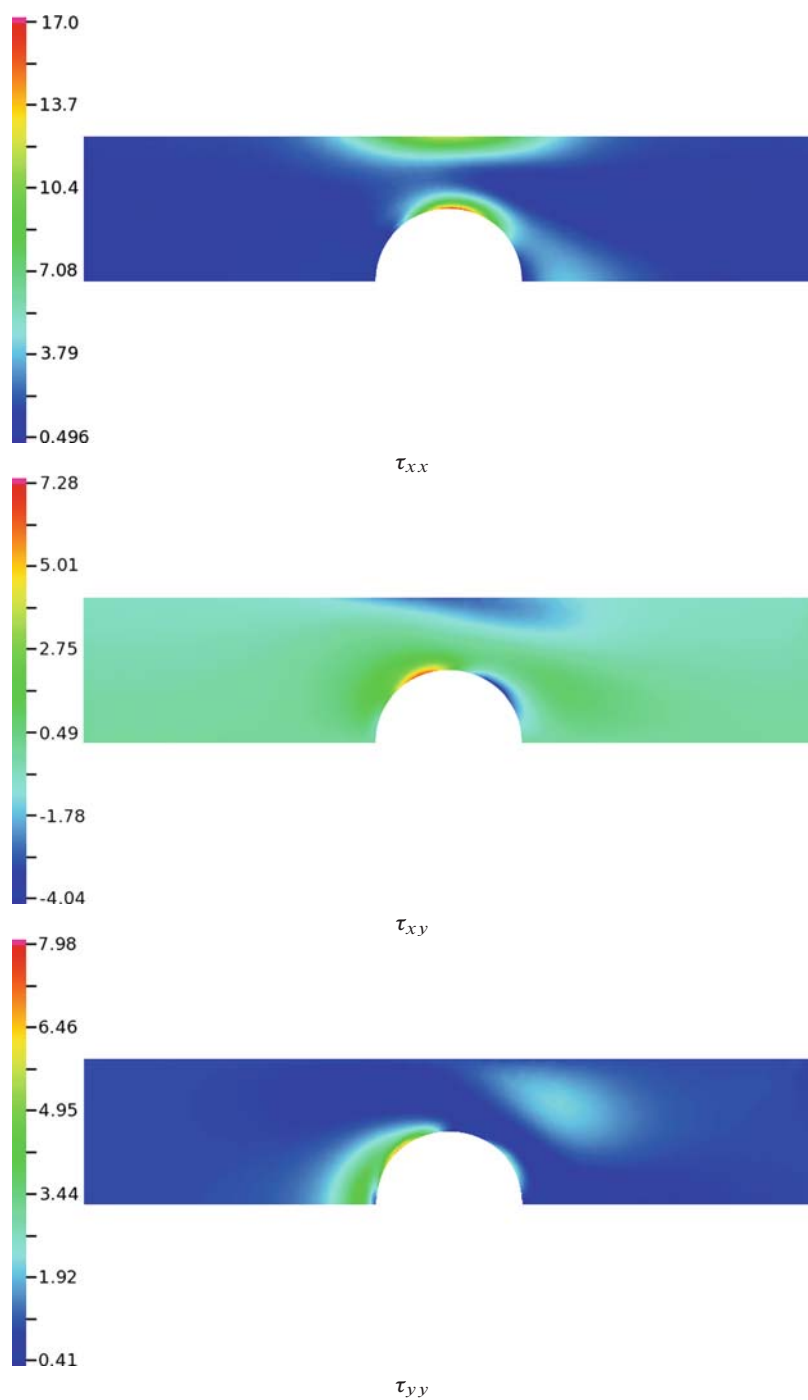


Fig. 1 The components of  $\underline{\tau}$  at  $T = 5$  for the  $Wi = 1$  case

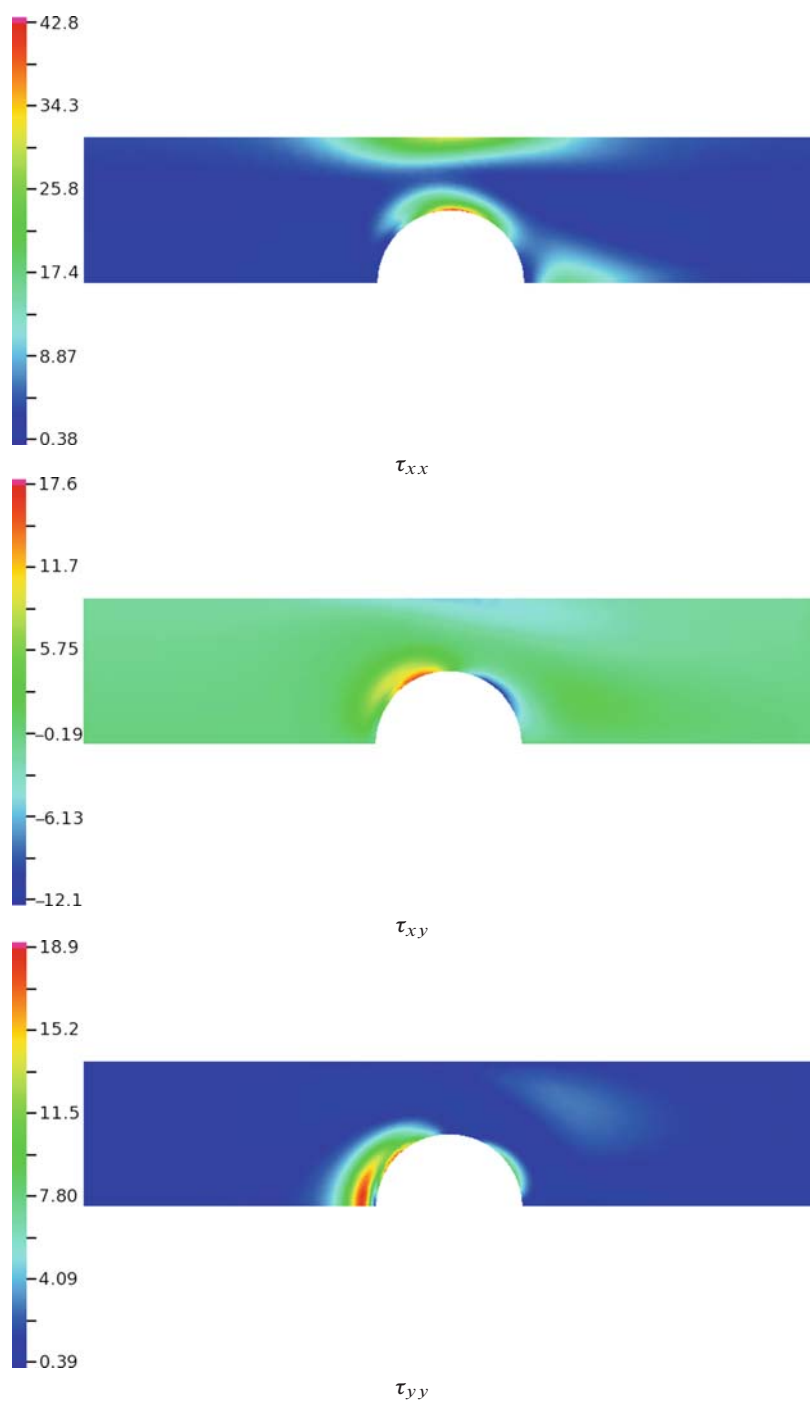


Fig. 2 The components of  $\underline{\tau}$  at  $T = 5$  for the  $Wi = 3$  case

Computational experimentation indicated that for both of these problems method II is significantly more efficient than method I (to the point where the semi-implicit method is computationally impractical), because, for the sake of stability, method I requires tighter restrictions on  $\Delta t$  and on the resolution of the discrete space  $\mathcal{P}_N(D)$  (cf. Sect. 2.6.2 of [13]). Thus, we only present numerical results for the fully-implicit scheme here; for a detailed comparison of the two methods for a model problem with a milder velocity field, see Sect. 5.1 of [14].

We solved case (1) using method II with  $(N_r, N_\theta) = (14, 14)$ , so that  $N_D = 406$  (recall that  $Q_\Omega$   $q$ -direction solves and  $N_D$   $x$ -direction solves are performed in each time-step of the alternating-direction algorithm). More spectral modes were required to resolve the solution in case (2) due to the larger Weissenberg number and hence we used  $(N_r, N_\theta) = (30, 30)$ , i.e.  $N_D = 1830$ , in that case. We took 500 time-steps of size  $\Delta t = 0.01$  and Figs. 1 and 2 show the components of  $\tilde{\tau}$  at  $T = 5$  in cases (1) and (2), respectively. These computations were performed on 80 processors of the Lonestar supercomputer at the Texas Advanced Computing Center (TACC), and took approximately 1.0 s per time-step in case (1) and 4.4 s per time-step in case (2) to perform.

## 5 Conclusions

We have summarised a range of results obtained in [14] and [15] for the analysis and implementation of numerical methods for solving the multiscale Navier–Stokes–Fokker–Planck system, which models the flow of dilute polymeric fluids. Most of our attention has been focused on the high-dimensional Fokker–Planck equation posed on the domain  $\Omega \times D$  in  $2d$  spatial dimensions. We developed an alternating-direction method for this equation that is efficient in practice and is also underpinned by rigorous numerical analysis.

We coupled this alternating-direction method to a mixed finite element method for the Navier–Stokes equations to obtain an algorithm for the coupled system (2)–(6). This algorithm was used to obtain computational results for a channel flow problem of physical interest. Parallel computation is particularly effective in the context of this problem because our alternating-direction solver for the high-dimensional Fokker–Planck equation is “embarrassingly parallel.”

## References

1. Balay, S., Buschelman, K., Eijkhout, V., Gropp, W. D., Kaushik, D., Knepley, M. G., McInnes, L. C., Smith, B. F., and Zhang, H. PETSc users manual. Tech. Rep. ANL-95/11 - Revision 2.1.5, Argonne National Laboratory, 2004.
2. Barrett, J. W., and Süli, E. Existence of global weak solutions to dumbbell models for dilute polymers with microscopic cut-off. *M3AS: Math. Model. Methods Appl. Sci.* 18, 6 (2008), 935–971.

3. Bird, R. B., Curtiss, C. F., Armstrong, R. C., and Hassager, O. *Dynamics of Polymeric Liquids, Volume 2, Kinetic Theory*, 2nd edn. Wiley, New York, 1987.
4. Chauvière, C., and Lozinski, A. Simulation of complex viscoelastic flows using Fokker–Planck equation: 3D FENE model. *J. Non-Newtonian Fluid Mech.* 122 (2004), 201–214.
5. Chauvière, C., and Lozinski, A. Simulation of dilute polymer solutions using a Fokker–Planck equation. *Comput. Fluids* 33 (2004), 687–696.
6. Douglas, J., and Dupont, T. Alternating-direction galerkin methods on rectangles. *Numerical Solution of Partial Differential Equations, II (SYNSPADE 1970)* (1971), 133–214.
7. Eisen, H., Heinrichs, W., and Witsch, K. Spectral collocation methods and polar coordinate singularities. *J. Comput. Phys.* 96, 2 (1991), 241–257.
8. Elman, H., Silvester, D., and Wathen, A. *Finite elements and fast iterative solvers*. Oxford Science Publications, Oxford, 2005.
9. Helzel, C., and Otto, F. Multiscale simulations of suspensions of rod-like molecules. *J. Comp. Phys.* 216 (2006), 52–75.
10. Jourdain, B., Lelièvre, T., and Le Bris, C. Existence of solution for a micro-macro model of polymeric fluid: the FENE model. *J. Funct. Anal.* 209, 1 (2004), 162–193.
11. Keunings, R. On the Peterlin approximation for finitely extensible dumbbells. *J. Non-Newtonian Fluid Mech.* 68 (1997), 85–100.
12. Kirk, B. S., Peterson, J. W., Stogner, R. M., and Carey, G. F. libmesh: A C++ library for parallel adaptive mesh refinement/coarsening simulations. *Eng. Comput.* 23, 3–4 (2006), 237–254.
13. Knezevic, D. J. Analysis and implementation of numerical methods for simulating dilute polymeric fluids. Ph.D. Thesis, University of Oxford, 2008. <http://www.comlab.ox.ac.uk/people/David.Knezevic/>.
14. Knezevic, D. J., and Süli, E. A heterogeneous alternating-direction method for a micro-macro model of dilute polymeric fluids. Submitted to M2AN, October 2008.
15. Knezevic, D. J., and Süli, E. Spectral galerkin approximation of Fokker–Planck equations with unbounded drift. Accepted to M2AN, October 2008. <http://web.comlab.ox.ac.uk/people/Endre.Suli/biblio.html>.
16. Kolmogorov, A. N. Über die analytischen Methoden in der Wahrscheinlichkeitsrechnung. *Math. Ann.* 104 (1931).
17. Lielens, G., Halin, P., Jaumain, I., Keunings, R., and Legat, V. New closure approximations for the kinetic theory of finitely extensible dumbbells. *J. Non-Newtonian Fluid Mech.* 76 (1998), 249–279.
18. Lozinski, A. Spectral methods for kinetic theory models of viscoelastic fluids. Ph.D. Thesis, École Polytechnique Fédérale de Lausanne, 2003.
19. Lozinski, A., and Chauvière, C. A fast solver for Fokker–Planck equation applied to viscoelastic flows calculation: 2D FENE model. *J. Comput. Phys.* 189 (2003), 607–625.
20. Lozinski, A., Chauvière, C., Fang, J., and Owens, R. G. Fokker–Planck simulations of fast flows of melts and concentrated polymer solutions in complex geometries. *J. Rheology* 47 (2003), 535–561.
21. Matsushima, T., and Marcus, P. S. A spectral method for polar coordinates. *J. Comput. Phys.* 120 (1995), 365–374.
22. Öttinger, H. C. *Stochastic Processes in Polymeric Fluids*. Springer, Berlin, 1996.
23. Owens, R. G., and Phillips, T. N. *Computational Rheology*. Imperial College Press, London, 2002.
24. Verkley, W. T. M. A spectral model for two-dimensional incompressible fluid flow in a circular basin I. Mathematical formulation. *J. Comput. Phys.* 136, 1 (1997), 100–114.
25. Warner, H. R. Kinetic theory and rheology of dilute suspensions of finitely extendible dumbbells. *Ind. Eng. Chem. Fundamentals* 11, 3 (1972), 379–387.
26. Zhou, Q., and Akhavan, A. A comparison of FENE and FENE-P dumbbell and chain models in turbulent flow. *J. Non-Newtonian Fluid Mech.* 109 (2003), 115–155.